Journal of Magnetism and Magnetic Materials 327 (2013) 110–120

Contents lists available at SciVerse ScienceDirect

Journal of Magnetism and Magnetic Materials

journal homepage: www.elsevier.com/locate/jmmm

Entanglement and quantum-classical crossover in the extended XX model with long-range interactions

M.W.V. Campelo [a], J.P. de Lima [a], L.L. Gonçalves [b,*]

[a] Departamento de Física, Universidade Federal do Piauí, Campus Ministro Petrônio Portela, 64049-550 Teresina, Piauí, Brazil
[b] Departamento de Engenharia Metalúrgica e de Materiais, Universidade Federal do Ceará, Campus do Pici, Bloco 714, 60455-760 Fortaleza, Ceará, Brazil

ARTICLE INFO

Article history:
Received 3 January 2012
Received in revised form
19 September 2012
Available online 4 October 2012

Keywords:
Extended XY model
Entanglement
Classical phase transition
Quantum phase transition

ABSTRACT

In this work we considered the one-dimensional extended isotropic XY model ($s=1/2$) in a transverse field with uniform long-range interactions among the z components of the spins. We studied the classical critical behaviour of the model through the behaviour of the magnetization, isothermal susceptibility, internal energy and specific heat. We have obtained exact expressions for these functions and evaluated the critical exponents. The phase diagrams for the classical critical behaviour were built for three cases of the multiplicity p of the multiple spin interaction, namely $p=2$, $p=3$ and $p\to\infty$. We have also shown that the quantum phase transitions can also be characterized through two quantifiers of entanglement, namely, the concurrence and the von Neumann entropy. We have also verified through the von Neumann entropy how the central charge of the model is affected by the multiplicity p, the coupling exchange J_2 and the uniform long-range interaction I.

0. Introduction

The studies on quantum phase transitions (QPT) [1] have been occupying an important place, not only from the experimental point of view but also from the theoretical one. In the last years, several works [2,3] have shown that the quantum critical point, at absolute zero, can deeply influence the properties of materials at finite temperatures. It has also been discovered that contrarily to what is expected for continuous transitions where there is a single-excitation energy scale associated with the slowing down of the order-parameter fluctuations which vanishes at the critical point, there can be additional energy scale excitations which vanish at the QPT as shown by Gegenwart et al. [4] for the antiferromagnet $YbRh_2Si_2$. Moreover, for magnetic materials, like $YbRh_2Si_2$, the phase diagram presents a "V" form shape for the dependence of the critical temperature as a function of the magnetic field, and inside this region the materials have an anomalous behaviour allowing us to formulate speculative interpretations like the ones presented in Ref. [3].

As an attempt to tackle this problem, some authors [5,6] have proposed different criteria in order to establish the border between the quantum and classical regimes. The study of this quantum-classical crossover is particularly welcome in exactly solvable one-dimensional spin chains in view of the accuracy of the results which can be obtained, and this has been one of the motivations for the present work. Although several factors, like pressure, concentration, disorder variation and magnetic field, can induce phase transitions in quantum systems in this work we will restrict our study to the quantum transitions which are induced by a transverse magnetic field.

QPT can also be studied through an impressive phenomenon, namely the quantum entanglement [7,8], which can be quantified in several ways. A comprehensive description of the state of art can be found in the review paper by Amico et al. [9] and references therein, and, in particular, the connection between the nonanalytical behaviour of the measure of quantum entanglement and QPT. In this work this connection is made through two measures of quantifying quantum entanglement, namely, concurrence [10,11] and von Neumann entropy [12]. For calculating the concurrence for spin chains, we need to obtain the two-site reduced density matrix, and we use the expression provided by Osborne and Nilsen [13] in their study about entanglement on transverse Ising model and the ground state of the XY model. Taking into account the symmetries of the Hamiltonian, we have obtained a two-site reduced density matrix, which is similar to the one found by Zhong and Tong [14] in their work about entanglement in the two-period XX model with long-range interactions. As in Zhong and Tong's work, the entries of reduced matrix depend on the correlation functions and the magnetization per site. The von Neumann entropy, or the block–block entanglement, for spin chains, is also used to characterize the QPT in the model we study here, and to analyze the universality

* Corresponding author.
E-mail address: lindberg@fisica.ufc.br (L.L. Gonçalves).

0304-8853/$ - see front matter © 2012 Elsevier B.V. All rights reserved.
http://dx.doi.org/10.1016/j.jmmm.2012.09.046

class near the critical point, by means of the central charge of the model [15,16]. By using conformal field theory, some authors [15–17] have shown that the block–block entanglement has a logarithmic singularity close to the critical points and that it depends on the central charge, which carries the universal characteristics of the model. To obtain the central charge and determine its universal behaviour is among the objectives of this work.

Therefore, in Section 1, we present the main results of the model, which has already been solved by Ribeiro et al. [18] and, in Section 2, we study its classical critical behaviour. On this section we also obtain the internal energy, the specific heat and some classical critical exponents, and present the phase diagrams for three cases of the multiplicity p. In Section 3 we determine the crossover lines by applying the criterion introduced by Gonçalves et al. [6] to establish the border between the quantum and classical regimes. In Section 4, we present the entanglement in the model and how it characterizes the QPT, and we also show how the central charge is affected by the interaction parameters of the model. Finally, in Section 5, we summarize the main conclusions of the paper.

1. The model and the main results

We consider the one-dimensional extended XX model ($s=1/2$) with uniform long-range interactions among the z components of the spins, whose Hamiltonian, by assuming periodic boundary conditions, is given by [18]

$$H=-J_1\sum_{j=1}^{N}(S_j^xS_{j+1}^x+S_j^yS_{j+1}^y)-h\sum_{j=1}^{N}S_j^z-\frac{I}{N}\sum_{j=1}^{N}\sum_{l=1}^{N}S_j^zS_l^z$$
$$-J_2\sum_{j=1}^{N}\sum_{\kappa=2}^{p}(S_j^xS_{j+\kappa}^x+S_j^yS_{j+\kappa}^y)S_{j+1}^zS_{j+2}^z\ldots S_{j+\kappa-1}^z, \tag{1}$$

where the parameters J_1, J_2 are the exchange couplings between nearest neighbours, I is the uniform long-range interaction among the z components, p is the multiplicity of the multiple spin interaction, h is the external magnetic field and N is the number of sites in the lattice, whose exact solution has been obtained by Ribeiro et al. [18]. The diagonalization of the Hamiltonian consists in using the Jordan–Wigner fermionization [19], followed by the Gaussian transformation and the Fourier transform, such that in the thermodynamic limit $N\to\infty$ which will be taken into account in all subsequent calculations, the functional of the Helmholtz free energy per site, obtained from the partition function, is given by [18]

$$f=\frac{h}{2}-\frac{k_BT}{\pi}\int_0^{\pi}\ln[1+\exp(\overline{\epsilon}_q(M^z))]\,dq+IM^z(1+M^z), \tag{2}$$

where

$$\overline{\epsilon}_q(M^z)\equiv\beta_T\epsilon_q(M^z), \tag{3}$$

with

$$\epsilon_q(M^z)=-\left[J_1\cos(q)+h+2IM^z+J_2\sum_{\kappa=2}^{p}\left(-\frac{1}{2}\right)^{\kappa-1}\cos(\kappa q)\right], \tag{4}$$

where q is the wave-vector, $\beta_T=1/k_BT$ and T is the temperature and the lattice parameter has been assumed to be equal to one. Following Ref. [18], we can obtain the state equation by imposing the stability conditions in Eq. (2), which is given by

$$M^z=\frac{1}{2\pi}\int_0^{\pi}\tanh\left(\frac{\overline{\epsilon}_q(M^z)}{2}\right)dq, \tag{5}$$

which, by redefining the interaction parameters in units of J_1, can be written in the form

$$M^z=\frac{1}{2\pi}\int_0^{\pi}\tanh\left(\frac{-\cos(q)-h-2IM^z-J\sum_{\kappa=2}^{p}\left(-\frac{1}{2}\right)^{\kappa-1}\cos(\kappa q)}{2\overline{T}}\right)dq, \tag{6}$$

where

$$J\equiv J_2,\quad \overline{T}\equiv k_BT. \tag{7}$$

We emphasize that we can treat the term $2IM^z$ in Eq. (6) as an additional external field, and we can define an effective field $h_{ef}=h+2IM^z$ which is appropriate for the study of the quantum-classical crossover presented in Section 2. This result comes from the fact that the long-range interaction, as pointed out by Suzuki [20], plays a role of an effective field in a system with short-range interactions.

2. Classical critical behaviour

For $I<0$ the system is totally frustrated and consequently does not present any classical critical behaviour. On the other hand, when $I>0$ the system undergoes first- and second-order transitions at finite temperature. To build the phase diagram of each case, for $\overline{T}>0$, we need to find the triple lines, which correspond to the interception of three surfaces of first-order transitions, and the critical lines corresponding to the classical second-order transitions. The triple lines can be found by solving the system

$$\begin{cases} M_{1t}^z-\frac{1}{2\pi}\int_0^{\pi}\tanh\left(\frac{\overline{\epsilon}_q(M_{1t}^z)}{2}\right)dq=0,\\ M_{2t}^z-\frac{1}{2\pi}\int_0^{\pi}\tanh\left(\frac{\overline{\epsilon}_q(M_{2t}^z)}{2}\right)dq=0,\\ M_{3t}^z-\frac{1}{2\pi}\int_0^{\pi}\tanh\left(\frac{\overline{\epsilon}_q(M_{3t}^z)}{2}\right)dq=0,\\ f(M_{1t}^z)-f(M_{2t}^z)=0,\\ f(M_{2t}^z)-f(M_{3t}^z)=0, \end{cases} \tag{8}$$

where $f(M_{it}^z)$ can be obtained from Eq. (2) and M_{it}^z's are the values of magnetization at the first-order transition.

The critical lines corresponding to second-order transitions can be obtained by requiring that the minimum of the Helmholtz free energy is triply degenerate. This means we need to solve the system

$$\begin{cases} M_{cr}^z-\frac{1}{2\pi}\int_0^{\pi}\tanh\left(\frac{\overline{\epsilon}_q(M_{cr}^z)}{2}\right)dq=0,\\ \frac{2\pi\overline{T}}{\alpha}-\int_0^{\pi}\operatorname{sech}^2\left(\frac{\overline{\epsilon}_q(M_{cr}^z)}{2}\right)dq=0,\\ \frac{\alpha^2}{\pi\overline{T}^2}\int_0^{\pi}\operatorname{sech}^2\left(\frac{\overline{\epsilon}_q(M_{cr}^z)}{2}\right)\tanh\left(\frac{\overline{\epsilon}_q(M_{cr}^z)}{2}\right)dq=0. \end{cases} \tag{9}$$

The above systems have been solved numerically for the cases $p=2$ with $J=2.5$, $p=3$ with $J=2$ and $p\to\infty$ with $J=-3$, which present the main features of the model.

In Fig. 1 we present the phase diagram for $p=2$ and $J=2.5$ with the classical and quantum first- and second-order transitions. The diagram also presents triple lines and the surfaces of first-order transitions.

We notice that the triple lines end at classical second-order lines, such that at this point, when $\overline{T}=0.166\ldots$, the system does not present three values of magnetization anymore, and the transition surface separates only two phases.

The phase diagram for the case $p=3$ with $J=2$ is shown in Fig. 2 and, finally, in Fig. 3, we present the phase diagram for the case $p\to\infty$ with $J=-3$. The important feature of this diagram is

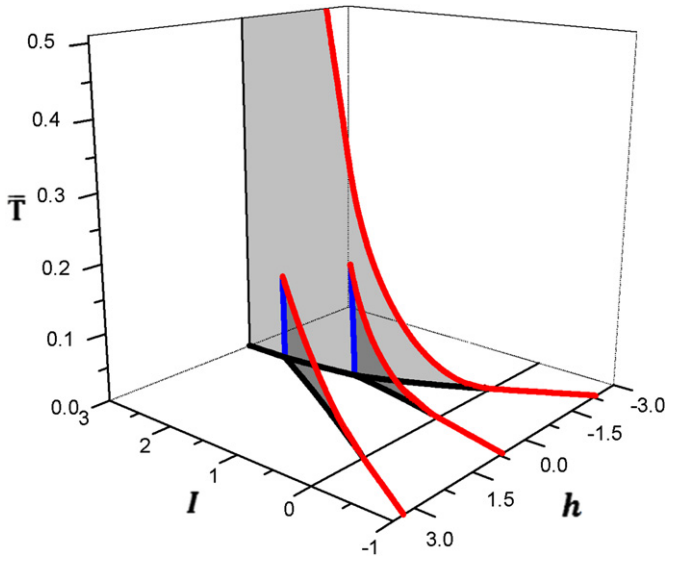

Fig. 1. Phase diagram for $p=2$ and $J=2.5$ is a function of I, h. The red lines correspond to classical second-order transitions, for $\overline{T}>0$, and second-order QPT for $\overline{T}=0$. The blue ones are the triple lines corresponding to first-order transitions, and the black lines correspond to first-order QPT. The gray regions are the surfaces of first-order transitions. (For interpretation of the references to colour in this figure legend, the reader is referred to the web version of this article.)

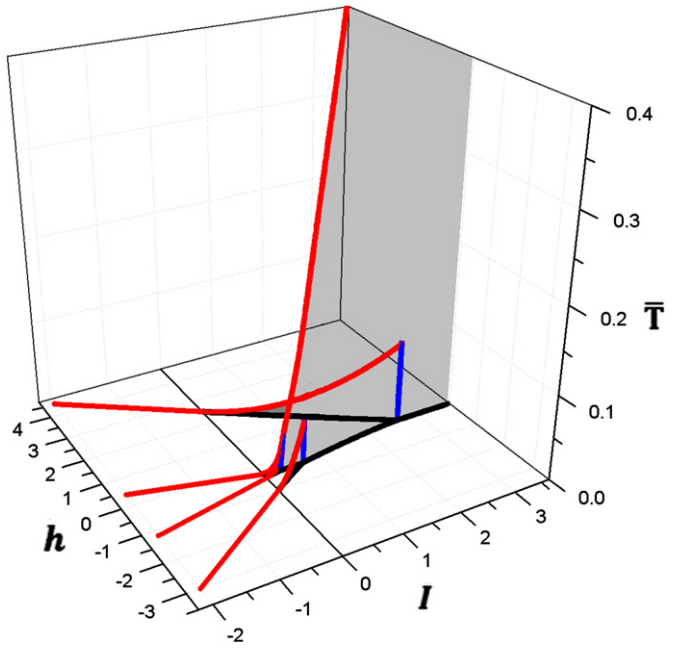

Fig. 2. Phase diagram for $p=3$ and $J=2$ as a function of I, h. The red lines correspond to second-order transitions, and the blue ones correspond to three triple lines. (For interpretation of the references to colour in this figure legend, the reader is referred to the web version of this article.)

the presence the mirror symmetry with respect to the magnetic field which is similar to the case $J=0$ [6].

We now evaluate the critical exponents for points of the critical lines in the case $\overline{T}>0$, and we will consider initially the case $p=2$ with $J=2.5$.

The exponent β associated to the induced magnetization is defined by

$$|M^z_{1t}-M^z_{2t}| = \widehat{M^z} \sim |\overline{T}-\overline{T}_c|^{\beta} \quad \text{when } \widehat{M^z}\to 0, \tag{10}$$

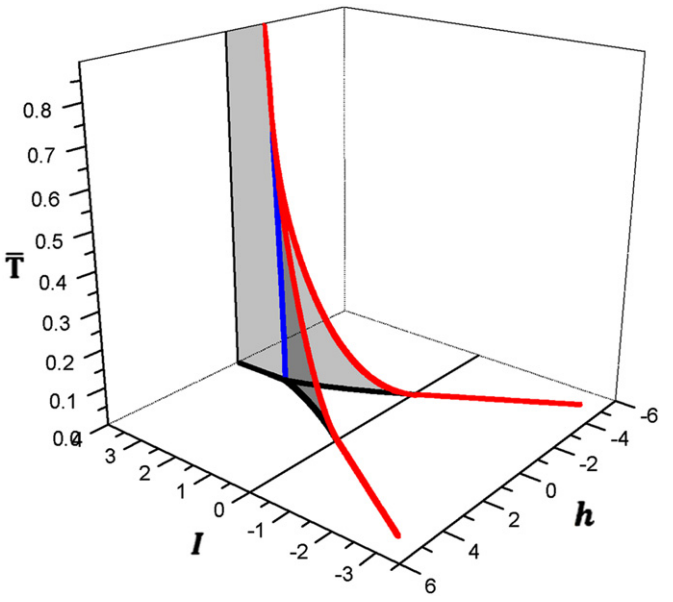

Fig. 3. Phase diagram for $p\to\infty$ and $J=-3$, as a function of I and h. The red lines correspond to second-order transitions, the blue one is a triple line where first-order transitions occur, and the black lines represent first-order QPT. The gray regions are also surfaces of classical first-order transitions. (For interpretation of the references to colour in this figure legend, the reader is referred to the web version of this article.)

where M^z_{1t} and M^z_{2t} are the values of the simultaneous magnetization on the first-order transition surface. This definition is analogous to the one for fluids [21], which is based on the difference between the densities of liquid and gaseous phases along the coexistence line which vanishes when we approach the critical point. For $p=2$, $I=2.24$, $h=0.156$ and at critical temperature $\overline{T}_c=0.11$, from the scaling behaviour of the magnetization shown in Fig. 4(a), we obtain $\beta=1/2$.

As expected, an identical result is obtained when we consider different values of the parameters. We have verified this result for $I=1.32$ and $h=-0.186$, where $\overline{T}_c$ is equal to 0.113.

The second critical exponent we evaluate is γ, which is associated to the isothermal susceptibility, and is given by

$$|\chi^{zz}_{\overline{T}}(M^z_{1t})-\chi^{zz}_{\overline{T}}(M^z_{2t})| \sim |\overline{T}-\overline{T}_c|^{-\gamma}, \tag{11}$$

where $\chi^{zz}_{\overline{T}}(M^z_{it})$ is the isothermal susceptibility as a function of the magnetization along the coexistence surface. It is obtained from Eq. (4) and is given by

$$\chi^{zz}_{\overline{T}} = \frac{\frac{1}{4\pi\overline{T}}\int_0^{\pi}\operatorname{sech}^2\left(\frac{\overline{\epsilon}_q}{2}\right)dq}{1-\frac{\alpha}{2\pi\overline{T}}\int_0^{\pi}\operatorname{sech}^2\left(\frac{\overline{\epsilon}_q}{2}\right)dq}. \tag{12}$$

For $p=2$ and at the same critical point, we show in Fig. 4(b) the difference between the isothermal susceptibilities versus $\overline{T}$ and in Fig. 4(c) its scaling behaviour, which leads to $\gamma=1/2$.

We find a similar behaviour at the critical point associated to the parameters $I=1.32$ and $h=-0.186$, which also leads to 1/2.

For $p=3$, the result for β and γ are identical to the previous ones and we have verified this result for different values of I and h. On the other hand, for $p\to\infty$ and $J<0$, the system presents two critical behaviours, namely, for $h\neq 0$ and $h=0$. An explicit result has been obtained for β by considering $J=-3$,$I=0.749$, $h=1.30$ and $\overline{T}_c=0.036$. The scaling region of the induced magnetization is shown in Fig. 5(a), and from this we find $\beta=1/2$.

For identical values of the parameters we find that the critical exponent γ, associated with the isothermal susceptibility whose scaling region is shown in Fig. 5(b), is equal to 1/2.

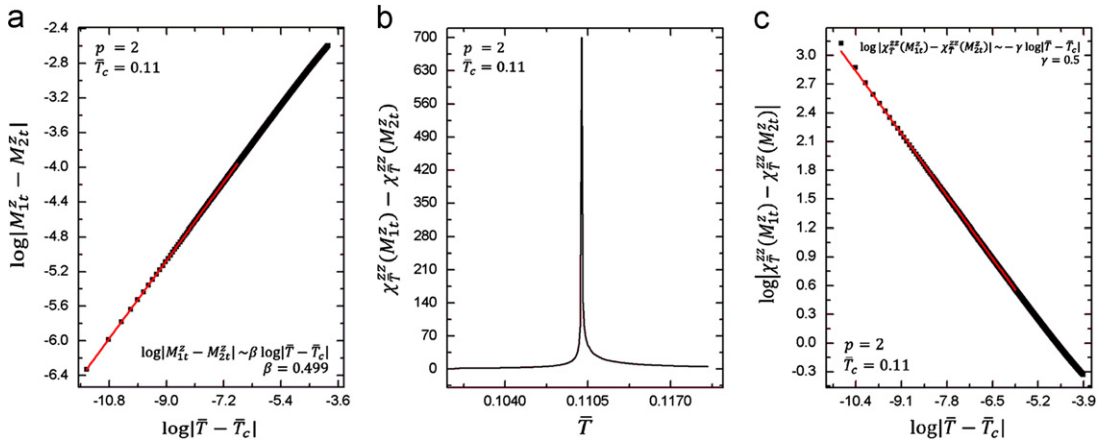

Fig. 4. (a) Scaling behaviour of the magnetization, (b) isothermal susceptibility and (c) scaling behaviour of the isothermal susceptibility as functions of temperature for $p=2$, $J=2.5$, $I=2.24$ and $h=0.156$, where $\overline{T}_c = 0.11$.

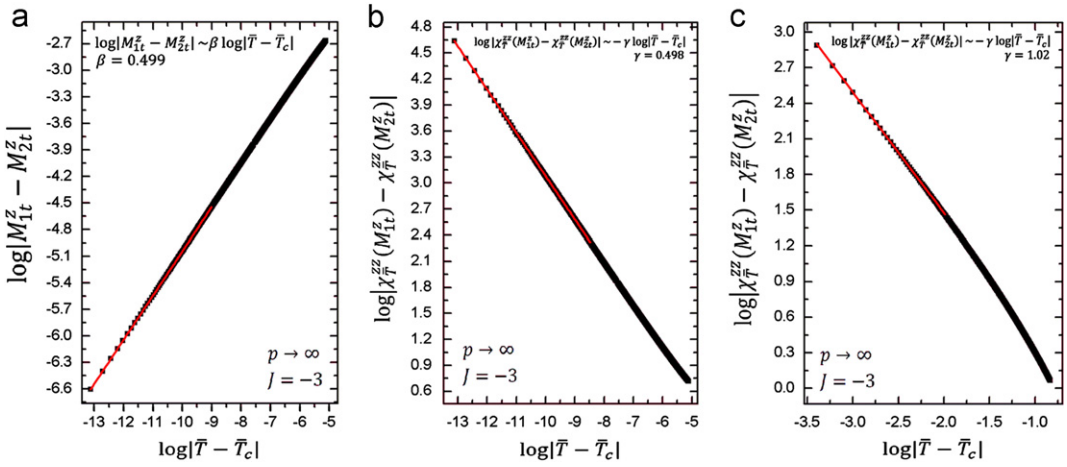

Fig. 5. (a) Scaling behaviour of the magnetization, (b) scaling behaviour of the isothermal susceptibility as functions of temperature for $p\to\infty$, $J=-3$, $I=0.749$ and $h=1.30$, where $\overline{T}_c = 0.036$. (c) Scaling behaviour of the isothermal susceptibility as a function of temperature for $p\to\infty$, $J=-3$, $I=2.87$ and $h=0$, where $\overline{T}_c = 0.877$.

However, for $h=0$, although we have found that the exponent β remains equal to 1/2, the exponent γ changes its value to 1. We have verified this result by considering $I=2.87$, with $\overline{T}_c = 0.877$, and the scaling region of the difference in the isothermal susceptibilities is presented in Fig. 5(c). This result shows that this model belongs to two different universality classes in a similar behaviour to the model studied by Gonçalves et al. for $J=0$ [6].

In order to further characterize the classical second-order transitions by the nonanalytical behaviour of other relevant thermodynamic functions like the specific heat, we need to obtain the internal energy ($u=U/N$), which is easily obtained from Eq. (2) and is given by

$$\frac{u}{J_1} = -IM^z(M^z+1) - \frac{h}{2} + \frac{1}{\pi}\int_0^{\pi} \frac{\epsilon_q dq}{1+e^{-\overline{\epsilon}_q(M^z)}}, \tag{13}$$

where $\overline{\epsilon}_q(M^z)$ and ϵ_q are given by Eqs. (3) and (4), respectively.

From Eq. (13), we can calculate the specific heat at constant field defined as

$$c_h = \left(\frac{\partial u}{\partial \overline{T}}\right)_h = -\frac{1}{k_B T^2}\left(\frac{\partial u}{\partial \beta_T}\right)_h, \tag{14}$$

which can be written in the form

$$c_h = \left\{\frac{1}{\pi k_B T^2}\int_0^{\pi}\left[\frac{(\epsilon_q(M^z))^2 e^{-\overline{\epsilon}_q(M^z)}}{(1+e^{-\overline{\epsilon}_q(M^z)})^2}\right] dq + \frac{2I}{\pi k_B T^3}\int_0^{\pi}\left[\frac{\epsilon_q(M^z)e^{-\overline{\epsilon}_q(M^z)}}{(1+e^{-\overline{\epsilon}_q(M^z)})^2}\left(\frac{\partial M^z}{\partial \beta_T}\right)_h\right] dq + \frac{I}{k_B T^2}(2M^z+1)\left(\frac{\partial M^z}{\partial \beta_T}\right)_h\right\}, \tag{15}$$

with $(\partial M^z/\partial\beta)_h$ obtained from Eq. (5) and given by

$$\left(\frac{\partial M^z}{\partial \beta_T}\right)_h = \frac{\frac{1}{4\pi\beta_T}\int_0^{\pi}[\overline{\epsilon}_q(M^z)]\,\mathrm{sech}^2\left(\frac{\overline{\epsilon}_q(M^z)}{2}\right) dq}{1-\frac{\alpha}{2\overline{T}\pi}\int_0^{\pi}\mathrm{sech}^2\left(\frac{\overline{\epsilon}_q(M^z)}{2}\right) dq}. \tag{16}$$

In Fig. 6(a) and (b) we present the internal energy and the specific heat as a function of the temperature for the case $p=2$ with $J=2.5$. At the point $\overline{T}_c = 0.11$, where the second-order transition occurs for the parameters $I=2.24$, $h=0.156$, the critical exponent α, defined by

$$c_h \sim |\overline{T} - \overline{T}_c|^{-\alpha}, \tag{17}$$

is equal to 1/2, as obtained from the scaling region shown in Fig. 6(c).

A similar result for α, $\alpha = 1/2$, is obtained at the point $\overline{T}_c = 0.113$ for the model when the parameters are $I=1.32$ and $h=-0.186$. An identical one is also obtained for the case $p=3$, independently of the parameter values.

For $p\to\infty$ with $J=-3$ the results are similar to the case $J=0$ studied by Gonçalves et al. [6] as already pointed out. In this case,

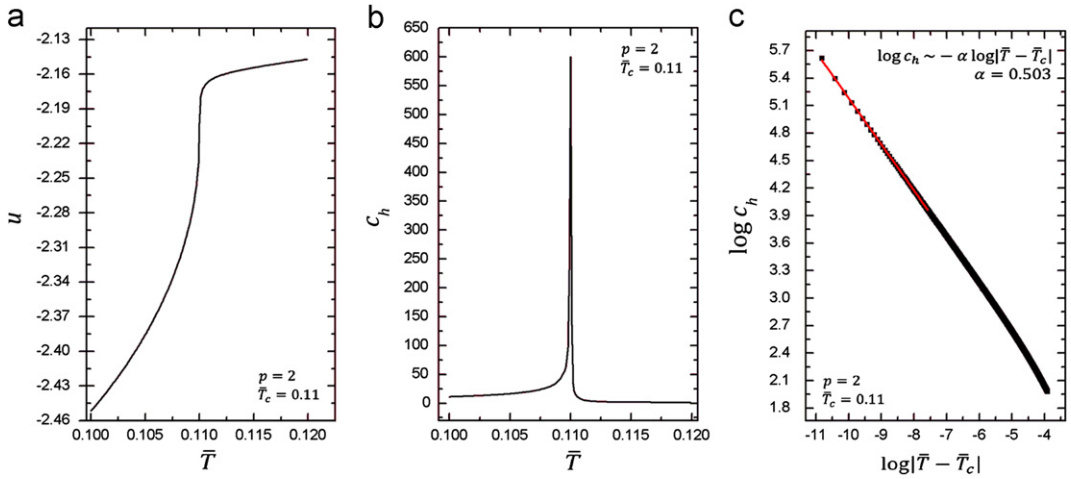

Fig. 6. (a) Internal energy, (b) specific heat and (c) scaling behaviour of the specific heat as functions of temperature for $p=2$, $J=2.5$, $I=2.24$ and $h=0.156$, where $\overline{T}_c=0.11$.

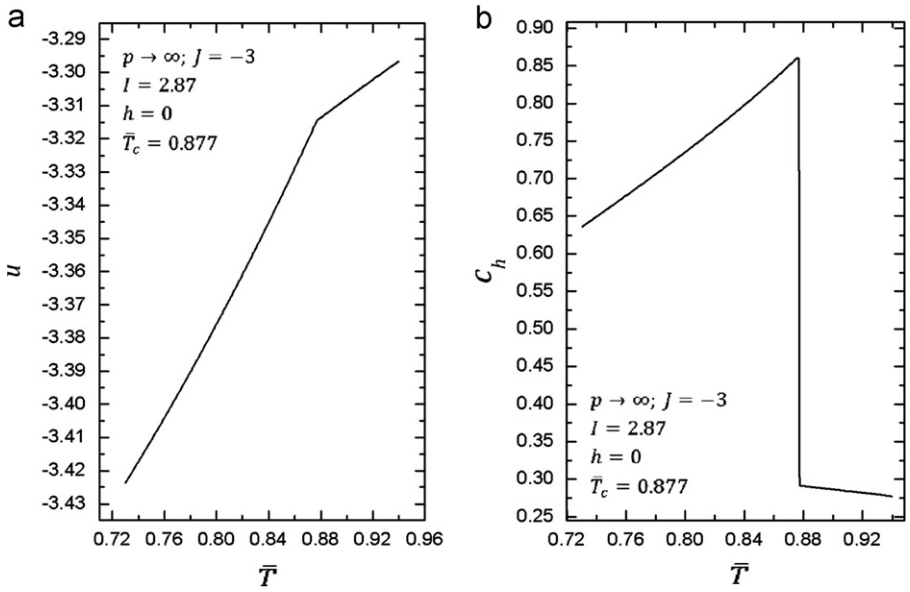

Fig. 7. (a) Internal energy and (b) specific heat as functions of the temperature for $p=\infty$, $J=-3$, $I=2.87$ and $h=0$. There is a classical second-order transition at $\overline{T}_c=0.877$.

for $h\neq 0$, the exponent α is identical to the one for $p=2$ and $p=3$, namely, $\alpha=1/2$, independently of the values of the other parameters. On the other hand, for $h=0$, from the behaviour of the internal energy and specific heat, around the critical point $\overline{T}_c=0.877$ for $I=2.87$ and $h=0$ shown in Fig. 7, we can conclude immediately that α is equal to zero confirming the change in the universality class which has already been pointed out.

It should be noted that the exponents α, β and γ obtained satisfy the Rushbrook scaling relation $\alpha+2\beta+\gamma=2$ [21].

3. Quantum-classical crossover

In this section we use the criterion proposed by Gonçalves et al. [6] to establish the border between quantum and classical regimes, namely, the crossover line which corresponds to the points of maxima of the magnetization as a function of temperature. By obtaining all these points we can build the crossover lines and display them as a function of the effective field $h_{ef}=h+2IM^z$, since the long-range interaction plays a role of an effective field in a system with nearest neighbour interactions, as pointed out by Suzuki [20].

A typical result is presented in Fig. 8, for $p=2$ and $J=2.5$ and $h=1.60$ where it is shown magnetization versus temperature for increasing values of h. For $h<h_t=0.723035\ldots$, where h_t is a transition field, the magnetization presents a maximum and this suggests that the quantum fluctuations dominate the thermal ones in the low temperature regime, whereas in the high temperature regime the thermal fluctuations dominate the quantum ones. For $h>h_t=0.723035\ldots.$ the magnetization presents a classical behaviour, since it decreases monotonically as a function of temperature.

The critical and crossover lines as functions of the effective field are shown in Figs. 9 and 10, corresponding to $p=2$ with $J=2.5$ and $p\to\infty$ with $J=-3$, respectively. The black lines represent the crossover lines, the red lines represent second-order transitions and the blue ones represent the triple lines where first-order transitions take place. In the regions marked with I we have the quantum regime, and in the regions marked with II we have the classical regime.

For $p=2$ and $J=2.5$, in Fig. 9, on the axis $\overline{T}=0$, the intervals $-1.632<\gamma_{ef}<-1.283$, $0.203<\gamma_{ef}<0.406$ and $2.2<\gamma_{ef}<2.402$, correspond to first-order QPT.

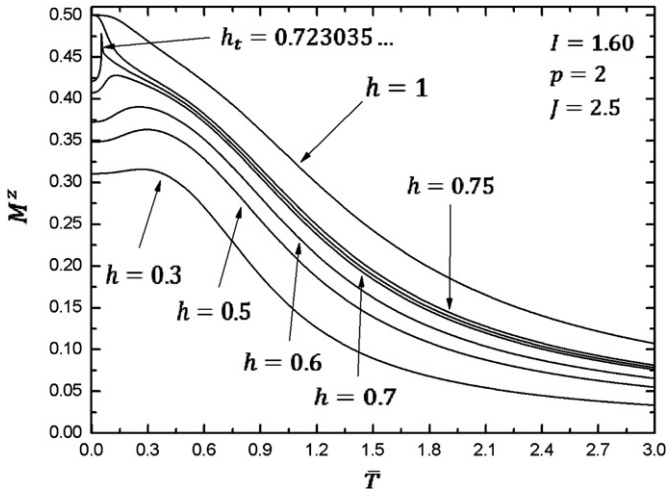

Fig. 8. Magnetization as a function of temperature for $I=1.60$ and different values of h. For $h<h_t$ the crossover points correspond to the maxima of the magnetization.

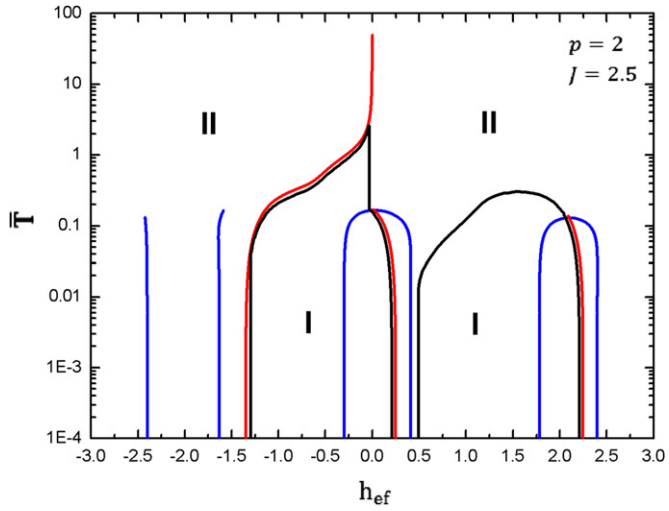

Fig. 9. Crossover lines for $p=2$ and $J=2.5$. The blue lines represent first-order transitions, the red ones represent classical second-order transitions and the black ones indicate the crossover line. The regions I correspond to the quantum regime and the regions II correspond to the classical regime. (For interpretation of the references to colour in this figure legend, the reader is referred to the web version of this article.)

For $p\to\infty$ and $J=-3$, in Fig. 10, on the axis $\overline{T}=0$, corresponding to $-2.546<\gamma_{ef}<-2$ and $2<\gamma_{ef}<2.546$, we have first-order QPT, similar to the results of Gonçalves et al. [6].

As it can be seen in Figs. 9 and 10, there are two and one crossover regions for $p=2$ and $p\to\infty$, respectively. It can also be shown that for $p=3$ there are three crossover regions. These results suggest that the number of crossover regions is identical to the number of spin liquid phases present in the model [18].

4. Quantum entanglement

The reduced density matrix of a pair of spins i and j takes the form

$$\rho_{ij} = \mathrm{tr}_{\widehat{ij}}(\rho) = \frac{1}{4}\sum_{\alpha,\beta=0}^{3} p_{\alpha\beta}\sigma_i^\alpha \otimes \sigma_j^\beta, \tag{18}$$

where $\sigma_i^0 = \hat{I}_i$ (unit matrix) and σ_i^α with $\alpha = 1,2,3$ represent the Pauli matrices, respectively σ_i^x, σ_i^y and σ_i^z and the coefficients $p_{\alpha\beta}$

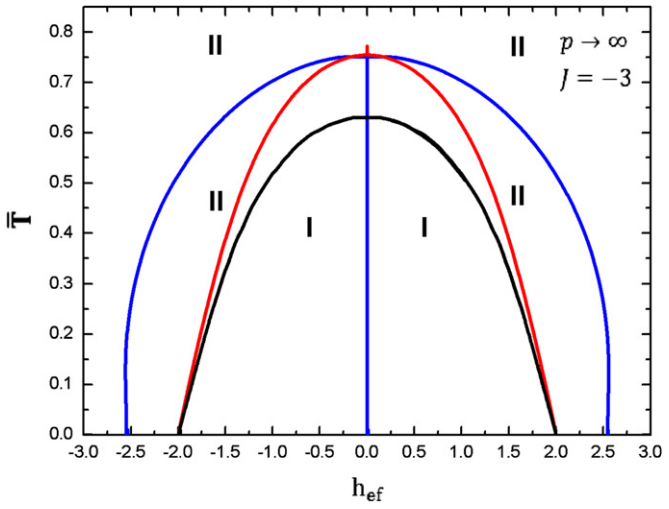

Fig. 10. Crossover lines for $p=\infty$ and $J=-3$. The blue lines represent first-order transitions, the red ones represent classical second-order transitions and the black ones indicate the crossover line. The regions I correspond to the quantum regime and the regions II correspond to the classical regime. (For interpretation of the references to colour in this figure legend, the reader is referred to the web version of this article.)

are determined by the relation

$$p_{\alpha\beta} = \mathrm{tr}(\sigma_i^\alpha \sigma_j^\beta \rho_{ij}) = \langle \sigma_i^\alpha \sigma_j^\beta \rangle. \tag{19}$$

If we know all the correlation functions we can completely build the reduced density matrix. However, we do not need to calculate all the 16 coefficients. This number can be reduced significantly by exploring the symmetries of the Hamiltonian, and it can be shown that the only non-vanishing coefficients are p_{00}, p_{11}, p_{22}, p_{33}, p_{03}, p_{30} [13,22]. From these results we can show that ρ_{ij} has the form

$$\rho_{ij} = \begin{pmatrix} u^+ & 0 & 0 & 0 \\ 0 & w_1 & z & 0 \\ 0 & z & w_2 & 0 \\ 0 & 0 & 0 & u^- \end{pmatrix}, \tag{20}$$

where

$$u^\pm = \tfrac{1}{4}(1 \pm 4M^z + 4\langle S_i^z S_j^z \rangle), \quad z = \langle S_i^x S_j^x \rangle + \langle S_i^y S_j^y \rangle,$$
$$w_1 = w_2 = \tfrac{1}{4}(1 - 4\langle S_i^z S_j^z \rangle), \tag{21}$$

and M^z is the magnetization per site. On deriving the expression of ρ_{ij}, we have used the fact that $[H,S^z]=0$, which implies that $\langle S_i^x S_j^x \rangle = \langle S_i^y S_j^y \rangle$.

The transversal correlation function $\langle S_i^z S_j^z \rangle$ is given by [18]

$$\langle S_m^z S_n^z \rangle = \left[\frac{1}{2\pi}\int_0^\pi \tanh\left(\frac{\overline{\epsilon}_q}{2}\right) dq\right]^2 - \left[\frac{1}{2\pi}\int_0^\pi \cos[q(m-n)] \tanh\left(\frac{\overline{\epsilon}_q}{2}\right) dq\right]^2 + \frac{\delta_{mn}}{4}. \tag{22}$$

The longitudinal correlation function $\langle S_j^x S_{j+r}^x \rangle$ is given by the Toeplitz determinant [18,19]

$$\langle S_j^x S_{j+r}^x \rangle = \frac{1}{4}\begin{vmatrix} \langle A_1 B_2 \rangle & \langle A_1 B_3 \rangle & \langle A_1 B_4 \rangle & \cdots & \langle A_1 B_{j+r+1} \rangle \\ \langle A_2 B_2 \rangle & \langle A_2 B_3 \rangle & \langle A_2 B_4 \rangle & \cdots & \langle A_2 B_{j+r+1} \rangle \\ \langle A_3 B_2 \rangle & \langle A_3 B_3 \rangle & \langle A_3 B_4 \rangle & \cdots & \langle A_3 B_{j+r+1} \rangle \\ \vdots & \vdots & \vdots & \ddots & \vdots \\ \langle A_j B_{j+r+2} \rangle & \langle A_j B_{l+3} \rangle & \langle A_j B_{l+4} \rangle & \cdots & \langle A_j B_{j+r+1} \rangle \end{vmatrix}, \tag{23}$$

where $\langle A_m B_n \rangle$ is given by [18,19]

$$\langle A_m B_n \rangle = -\frac{1}{\pi}\int_0^{\pi} \cos[q(m-n)] \tanh\left(\frac{\overline{\epsilon}_q(M^z)}{2}\right) dq. \quad (24)$$

By using the above results, we obtain the concurrence between two spins i and j which is defined by [11]

$$C_{ij} = \max\{\lambda_1 - \lambda_2 - \lambda_3 - \lambda_4, 0\}, \quad (25)$$

where $\lambda_1 > \lambda_2 > \lambda_3 > \lambda_4$ are the square roots of the eigenvalues of the operator

$$R_{ij} = \rho_{ij}(\sigma^y \otimes \sigma^y)\rho_{ij}^*(\sigma^y \otimes \sigma^y), \quad (26)$$

which in terms of $u^{\pm}$, z, w_1 and w_2, the square roots of the eigenvalues of the operator R_{ij} are given by

$$\lambda_{1,2} = \pm\sqrt{u^+ u^-} \quad \text{and} \quad \lambda_{3,4} = z \pm w_1. \quad (27)$$

$C_{ij} = 0$ corresponds to an unentangled state and $C_{ij} = 1$ to a completely entangled state.

The signature of the QPT is present in the concurrence nonanalytical behaviour which occurs at the transition points [13]. This can be seen in Fig. 11, where we present the magnetization and the concurrence as functions of the magnetic field, at $T=0$, and in Fig. 12, where we present the derivative of the concurrence with respect to the magnetic field and the isothermal susceptibility as functions of the magnetic field, also at $T=0$, for $p=2$, $J=2.5$ and different values of I. It should be noted that for $I=2.4$, the concurrence is zero since

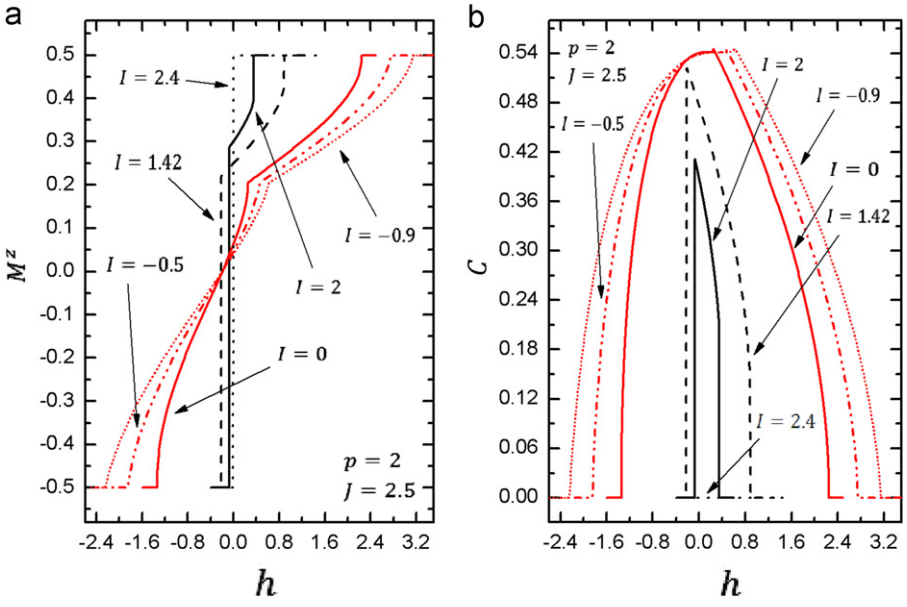

Fig. 11. (a) Magnetization and (b) concurrence (as functions of the magnetic field at $\overline{T} = 0$, for $p=2$, $J=2.5$ and different values of I. The red lines correspond to second-order QPT and the black ones refer to first-order QPT. For $I=2.4$ the systems collapse in a single ferromagnetic phase. (For interpretation of the references to colour in this figure legend, the reader is referred to the web version of this article.)

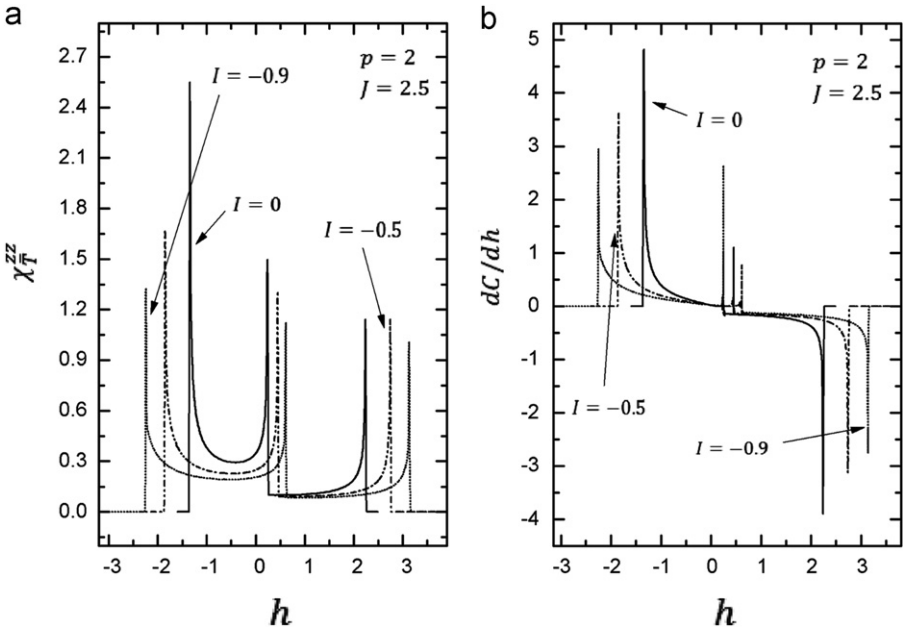

Fig. 12. (a) Isothermal susceptibility and (b) $dC/d\gamma$ as functions of the magnetic field at $\overline{T} = 0$, for $p=2$, $J=2.5$ and different values of I. The divergence in the figures corresponds to second order QPT.

the two ferromagnetic phases collapse in a single phase, which corresponds to a degenerate ferromagnetic state.

Similar results can be obtained for $p\to\infty$, which are shown in Figs. 13 and 14 for $J=-3$ and different values I.

The QPT can be also characterized by means of the von Neumann entropy or the block–block entanglement, which corresponds to the entanglement of a block of L contiguous spins and the rest of the chain, and is defined as [12]

$$S_L \equiv -\mathrm{tr}(\rho_L \log_2 \rho_L), \tag{28}$$

where ρ_L is the reduced density matrix for L contiguous spins. S_L can also be given by the expression [14]

$$S_L = -\sum_{n=1}^{L}[(1-\lambda_n)\log_2(1-\lambda_n)+\lambda_n \log_2 \lambda_n], \tag{29}$$

where λ_n are the eigenvalues of the matrix

$$G_L = \begin{pmatrix} g_{1,1} & g_{1,2} & \cdots & g_{1,L} \\ g_{2,1} & g_{2,2} & \cdots & g_{2,L} \\ \vdots & \vdots & \ddots & \vdots \\ g_{L,1} & g_{L,2} & \cdots & g_{L,L} \end{pmatrix}, \tag{30}$$

and $g_{i,j} = \langle c_i^{\dagger} c_j \rangle$ can be calculated by using Wick's [24] theorem and, for the model studied here, is given by the expression

$$g_{i,j} = \frac{1}{2}\left\{\delta_{ij} + \frac{1}{\pi}\int_0^{\pi} \cos[q(i-j)]\tanh\left(\frac{\overline{\epsilon}_q(M^z)}{2}\right) dq\right\}. \tag{31}$$

The block–block entanglement as a function of h is shown in Fig. 15(a), for $p=2$ with $J=2.5$ and $I=-0.9$, -0.5, 0, 1.42, 2 and 2.4, where the first- and second-order QPT can be seen.

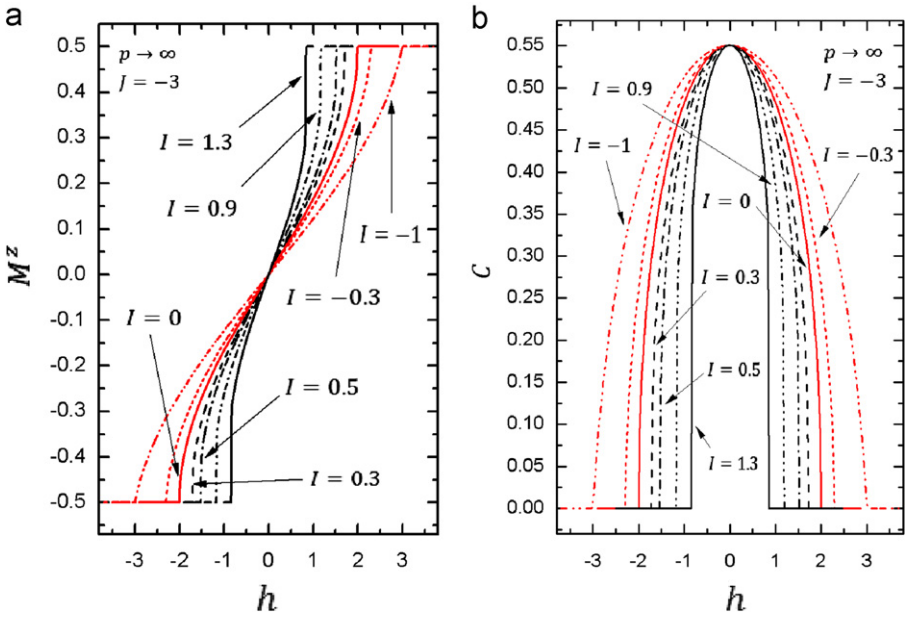

Fig. 13. Magnetization (a) and concurrence (b) as a function of the magnetic field at $\overline{T}=0$, for $p=\infty$, $J=-3$ and different values of I. The red lines correspond to second-order QPT and the black ones refer to first-order QPT. (For interpretation of the references to colour in this figure legend, the reader is referred to the web version of this article.)

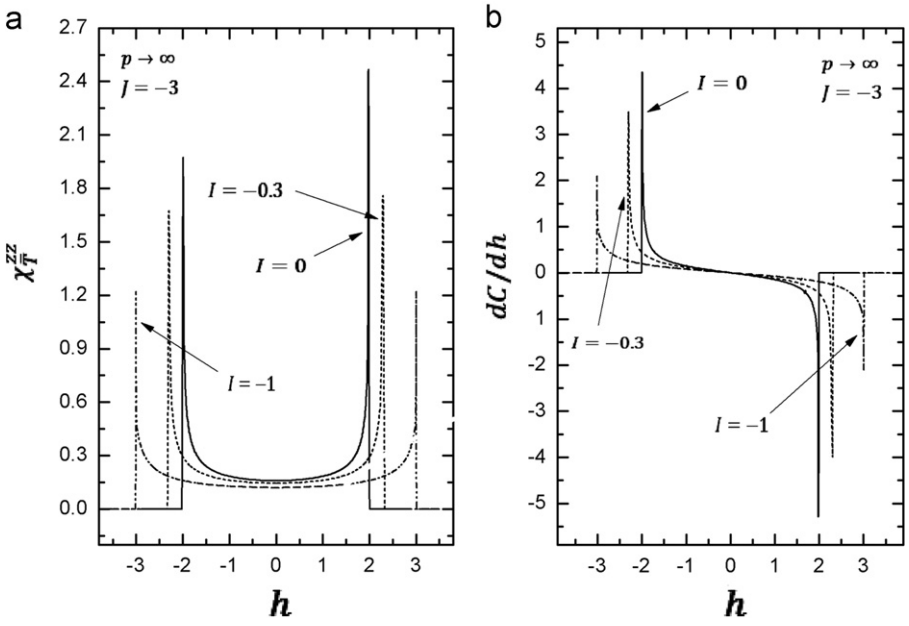

Fig. 14. Isothermal susceptibility (a) and $dC/d\gamma$ (b) as a function of the magnetic field at $\overline{T}=0$, for $p=\infty$, $J=-3$ and different values of I. The divergences in the figures correspond to second order QPT.

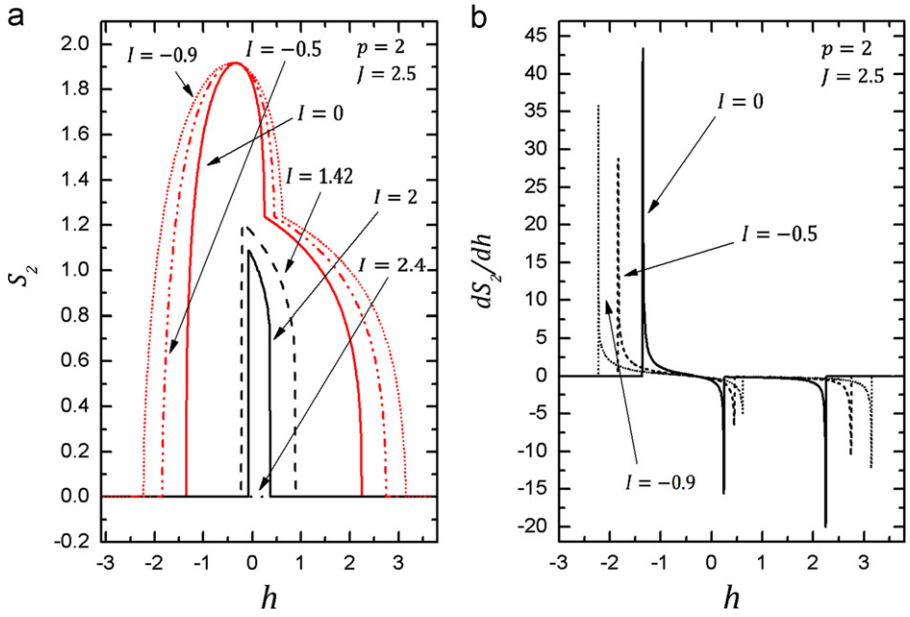

Fig. 15. (a) Block–block entanglement and (b) $dS_2/d\gamma$ as functions of the magnetic field at $\overline{T}=0$, for $p=2$, $J=2.5$, and different values of I. The black lines in (a) correspond to first-order QPT and the red ones to second-order QPT. The divergences in (b) correspond to second-order QPT. (For interpretation of the references to colour in this figure legend, the reader is referred to the web version of this article.)

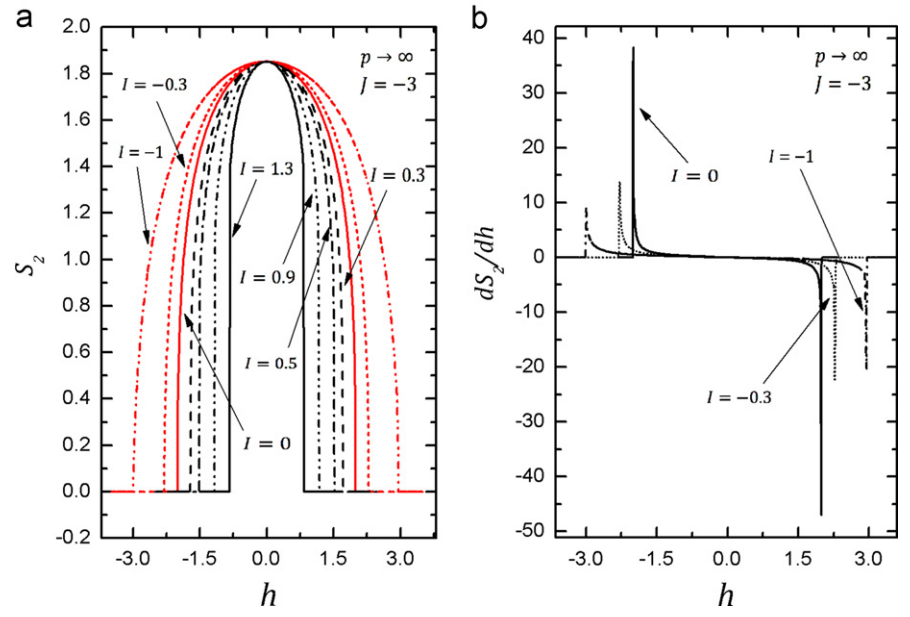

Fig. 16. (a) Block–block entanglement and (b) $dS_2/d\gamma$ as functions of the magnetic field at $\overline{T}=0$, for $p\to\infty$, $J=-3$, and different values of I. The black lines in (a) correspond to first-order QPT and the red ones to second-order QPT. The divergences in (b) correspond to second-order QPT. (For interpretation of the references to colour in this figure legend, the reader is referred to the web version of this article.)

For the same set of parameters, the divergences of dS_2/dh which occur at the second-order QPT are shown in Fig. 15(b).

The results for $p\to\infty$, with $J=-3$, are shown in Fig. 16(a) and (b) for block–block entanglement and for dS_2/dh, respectively. They present the main features of the quantum critical behaviour already discussed, although in this case, the block–block entanglement is symmetric with respect to the axis $h=0$ and dS_2/dh is antisymmetric.

The block–block entanglement, for closed spin chains where we have periodic boundary conditions and near the critical points, presents a scaling form on the number of sites in the lattice, which is also a signature of the critical behaviour, which has the form [15–17,23]

$$S_L = \frac{c}{3}\log\left(\frac{L}{a}\right) + k, \tag{32}$$

where L refers to a block of L contiguous spins in the lattice, a is the lattice spacing, c is the central charge of the conformal field theory and k is a non-universal constant. For $I=0$, the central charge does not depend on J and p, and is equal to one. This can be seen in Figs. 17(a) and (b), for $p=2$, and in Fig. 17(c) and (d), for $p=3$ and $p\to\infty$, respectively, where we have plotted S_L versus

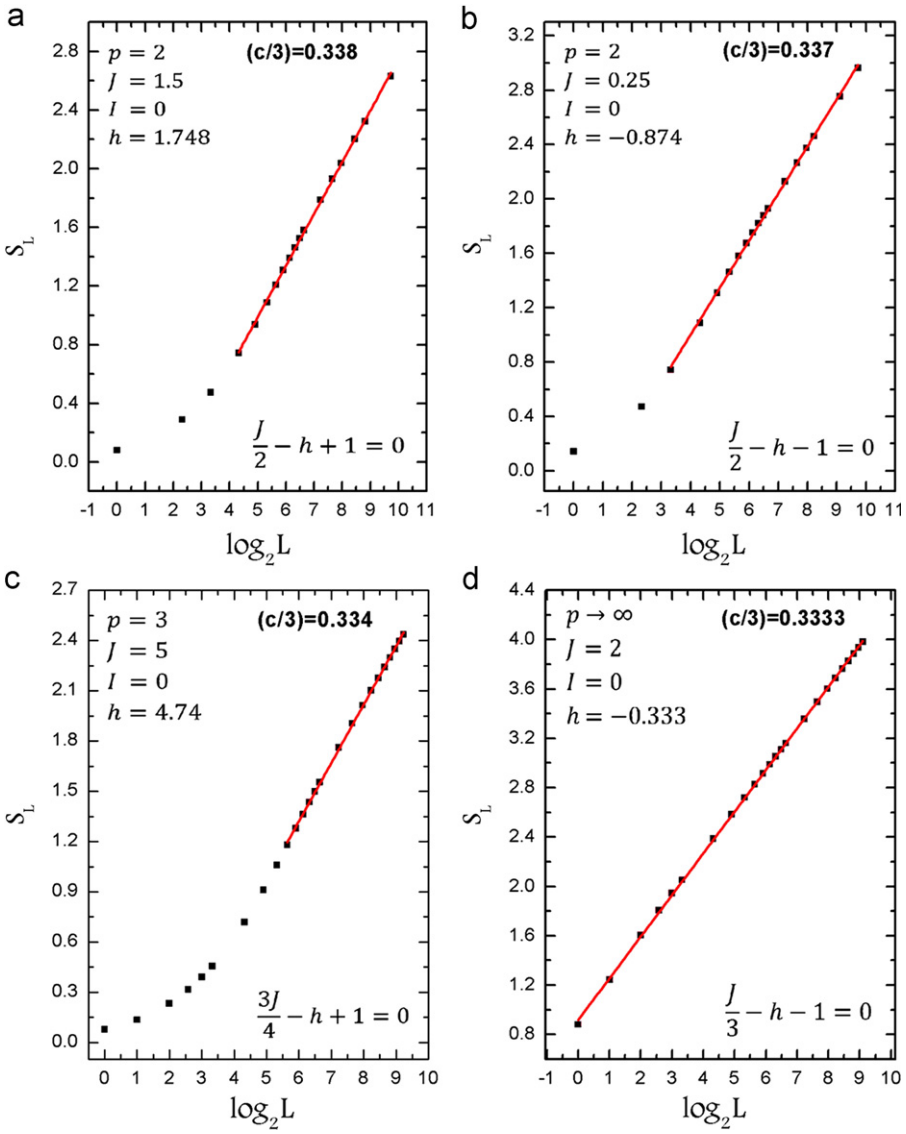

Fig. 17. Scaling behaviour of the von Neumann entropy as a function of the size L of the block at $\overline{T}=0$: (a) for $p=2$,$I=0$, $h=1.748$ and $J=1.5$, (b) for $p=2$, $I=0$, $h=-0.874$ and $J=0.25$, (c) for $p=3$, $I=0$, $h=4.74$ and $J=5$ and (d) for $p\to\infty$, $I=0$, $h=-0.333$ and $J=2$.

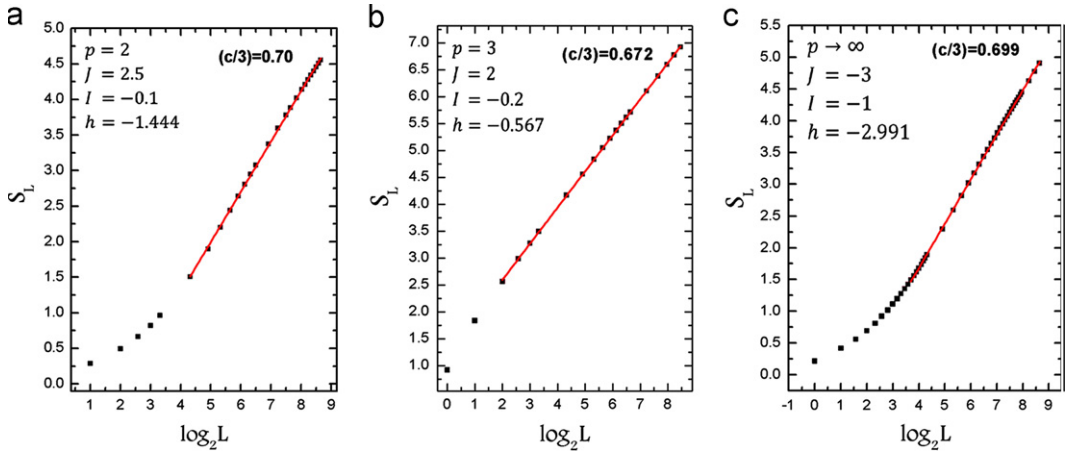

Fig. 18. Scaling behaviour of the von Neumann entropy as a function of the size L of the block at $\overline{T}=0$: (a) for $p=2$, $I=-0.1$, $h=-1.444$ and $J=2.5$, (b) for $p=3$, $I=-0.2$, $h=-0.567$ and $J=2$ and (c) for $p\to\infty$, $I=-1$, $h=-2.991$ and $J=-3$.

$\log_2 L$ for values of h near to the critical points. Therefore, the central charge is a universal constant in the model, and is identical to the value obtained for XX model [25].

For $I\neq 0$, the central charge *also* does not depend on J and p, and is equal approximately to 2.1. This can be seen in Fig. 18(a) for $p=2$, in Fig. 18(b) for $p=3$ and in Fig. 18(c) for $p\to\infty$, where we have also

plotted S_L versus $\log_2 L$ for values of h near to the critical points, and consequently we can conclude that central charge does depend on the long-range interaction only, which confirms the results of Ribeiro et al. for the case $p=2$ [18].

5. Conclusions

In this work we have considered the one-dimensional XX model with multiple spin interactions and uniform long-range interactions among the z components of the spins, in a transverse magnetic field. We have used the Helmholtz free energy and the equation of state obtained by Ribeiro et al. [18] to study the classical critical behaviour of the model for the cases $p=2$ with $J=2.5$, $p=3$ with $J=2$ and $p\to\infty$ with $J=-3$. We have obtained expressions for the induced magnetization, isothermal susceptibility, internal energy and specific heat and determined the phase diagrams for the mentioned cases. We have also evaluated the critical exponents α, β and γ for points along the critical lines, and it has been verified that they satisfy the Rushbrook relation $\alpha+2\beta+\gamma=2$ [21]. It has also been shown that the classical critical behaviour of the model model belongs to two different universality classes. The crossover lines have been found for these three cases and the presence of three crossover regions in the case $p=3$, two regions for the case $p=2$ and one for the case $p\to\infty$, which suggests that the number of crossover regions is identical to the number of spin liquid phases [18]. We have also characterized the QPT of the model through two measurements of entanglement, namely, the concurrence and the block–block entanglement, and we have used the last one to verify which parameters p, J and I affect the central charge of the model. Based on our results, we have concluded that the long-range interaction I is the only responsible for changing the central charge, and consequently the universality class of the quantum critical behaviour of the model, in accordance with Ribeiro et al. results for $p=2$ [18].

Acknowledgements

The authors would like to thank the Brazilian Agencies Conselho Nacional de Desenvolvimento Científico e Tecnológico (CNPq), Coordenação de Aperfeiçoamento de Nível Superior (CAPES) and Fundação de Amparo à Pesquisa do Estado do Pauí (FAPEPI) for partial financial support. They would also like to thank the anonymous referees for their valuable comments.

References

[1] S. Sachdev, Quantum Phase Transitions, Cambridge, 1999.
[2] P. Coleman, A.J. Schofield, Nature 433 (2005) 226.
[3] A.J. Schofield, Science 315 (2007) 945.
[4] P. Gegenwart, T. Westerkamp, K. Kreliner, Y. Tokiwa, S. Paschen, C. Geibel, F. Steglich, E. Abrahams, Q. Si, Science 315 (2007) 969.
[5] K. Fabricius, B.M. McCoy, Physical Review B 59 (1999) 381.
[6] L.L. Gonçalves, L.P.S. Coutinho, J.P. de Lima, Physica A 345 (2005) 71.
[7] A. Einstein, B. Podolsky, N. Rosen, Physical Review 47 (1935) 777.
[8] N. Bohr, Physical Review 48 (1935) 696.
[9] L. Amico, R. Fazio, A. Osterloh, V. Vedral, Reviews of Modern Physics 80 (2008) 517.
[10] S. Hill, W.K. Wootters, Physical Review Letters 78 (1997) 5022.
[11] W. Wootters, Physical Review Letters 80 (1998) 2245.
[12] C.H. Bennett, H. Bernstein, S. Popescu, B. Schumacher, Physical Review A 53 (1996) 2046.
[13] T. Osborne, M. Nielsen, Physical Review A 66 (2002) 032110.
[14] M. Zhong, P. Tong, Journal of Physics A: Mathematical and Theoretical 42 (2009) 355002.
[15] P. Calabrese, J. Cardy, International Journal of Quantum Information 4 (2006) 429–438.
[16] P. Calabrese, J. Cardy, Journal of Statistical Mechanics P06002 (2004).
[17] P. Calabrese, J. Cardy, B. Doyon, Journal of Physics A: Mathematical and Theoretical 42 (2009) 500301.
[18] F.G. Ribeiro, J.P. de Lima, L.L. Gonçalves, Journal of Magnetism and Magnetic Materials 323 (2011) 39–50.
[19] E. Lieb, T. Schultz, D. Mattis, Annals of Physics, NY 16 (1961) 407.
[20] M. Suzuki, Journal of the Physical Society of Japan 21 (1966) 2140.
[21] H.E. Stanley, Introduction to Phase Transitions and Critical Phenomena, Oxford, 1987.
[22] T. Deguchi, P.K. Ghosh, Journal of Physics A: Mathematical and Theoretical 42 (2009) 475208.
[23] A. Osterloh, L. Amico, G. Falci, R. Fazio, Nature 416 (2002) 608.
[24] R.D. Mattuck, A Guide to Feynman Diagrams in the Many-Body Problem, Dover Publications, 1992.
[25] G. Vidal, J. Latorre, E. Rico, A. Kitaev, Physical Review Letters 90 (2003) 227902.